LA-UR-01-4185
Approved for public release; distribution is unlimited.

Title: NEW GEANT SIMULATIONS OF NEUTRON CAPTURE EXPERIMENTS DETECTOR WITH A 4π BaF_2

Author(s): R. Reifarth, M. Heil, F. Kaeppeler, F. Voss, K. Wisshak, R. C. Haight, M. R. Dragowsky, M. M. Fowler, R. S. Rundberg, J. L. Ullmann, J. B. Wilhelmy and E. H. Seabury

Submitted to:

NEW GEANT SIMULATIONS OF NEUTRON CAPTURE EXPERIMENTS WITH A 4π BaF_2 DETECTOR

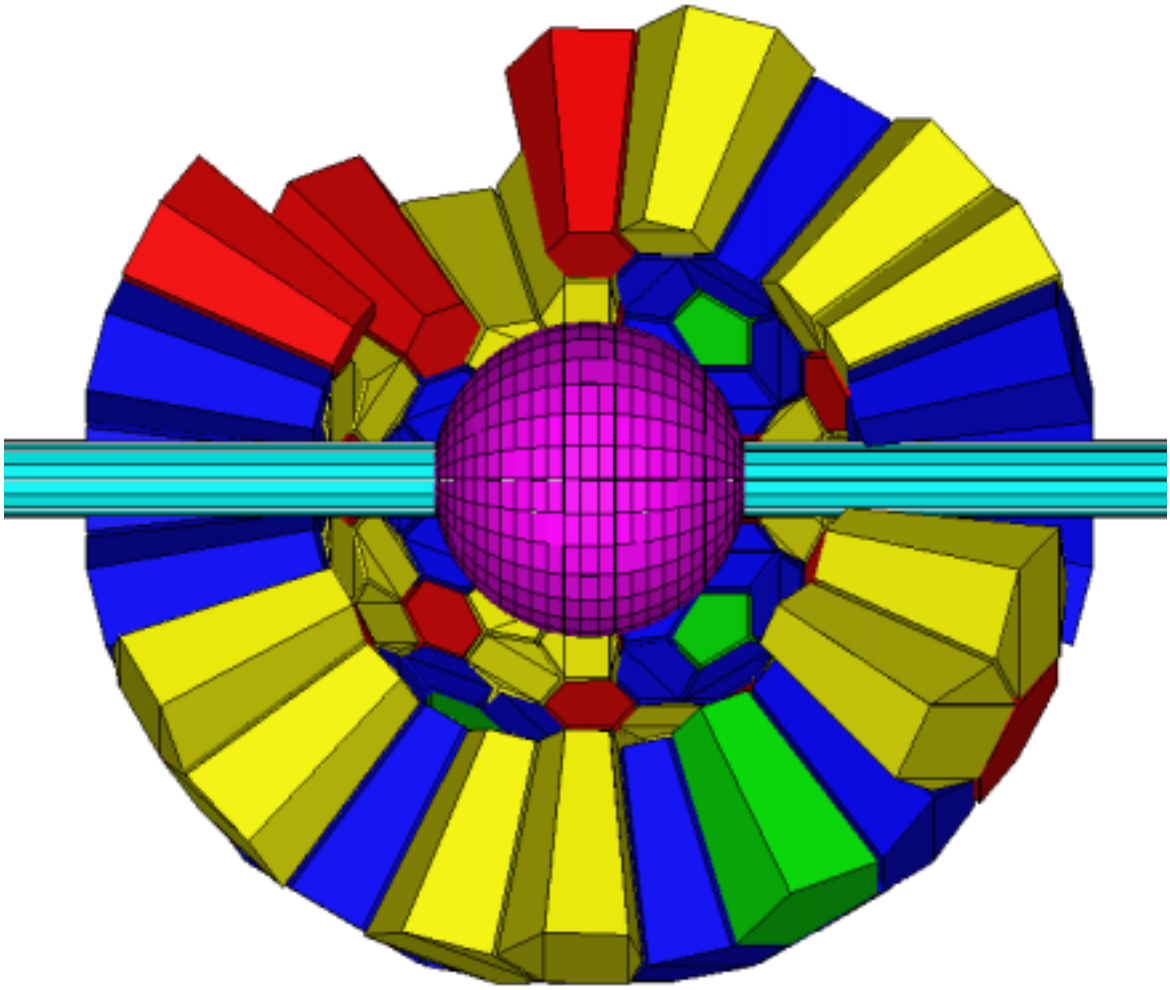

R. Reifarth, M. Heil, F. Kaeppeler, F. Voss, K. Wisshak
Forschungszentrum Karlsruhe

R. C. Haight, M. R. Dragowsky, M. M. Fowler,
R. S. Rundberg, J. L. Ullmann, J. B. Wilhelmy
Los Alamos National Laboratory

E. H. Seabury
Idaho National Engineering and Environmental Laboratory

July 2001

Table of Contents

List of Figures

List of Tables

1 Introduction

The goal of this project is to give updated information useful for the final design of a γ-ray detector to investigate neutron capture (n, γ) reactions on radioactive nuclei at the Manuel Lujan Jr. Neutron Scattering Center (MLNSC) moderated neutron source at LANSCE. This report is a continuation of the reports by Heil et al. [Hei99], [Hei01].

Data for neutron energies from 1 eV up to approximately 10 MeV are desired. The radioactive nuclei can have half-lives as short as a few months. With the sample sizes foreseen, typically 1 mg, the radioactive decay rate can exceed tens of Curies (Ci). Many of the nuclei of interest emit copious quantities of energetic γ-rays, which generally have significantly less energy (<3 MeV almost always) than the sum energy of gamma rays following neutron capture (~ 6 MeV), but the possibility exists that several gamma rays from unrelated radioactive decays could occur nearly simultaneously and thereby be difficult to separate from the neutron-capture γ-rays.

In addition to the capture γ-rays and radiation from the radioactive decay, the detector will also be subjected to neutrons scattered from the sample and, if the shielding is not perfect, also to background neutrons. The sensitivity of the detector to scattered neutrons must therefore also be assessed.

This design for the DANCE γ-ray detector array is intended to address the experimental challenges discussed above. So that the neutron capture rate is not overwhelmed by the radioactive decay rate, the intense neutron source at MLNSC is chosen. A very reasonable capture rate can then be achieved with a small sample (about 1 mg) of the radioisotope. A design that would accept even smaller samples is a continuing goal. To reduce the sensitivity to scattered neutrons, the materials of the detector should have small neutron capture cross sections. The detector is highly segmented so that the counting rate in a single element is acceptable. For this reason, we choose a 162 element, "soccer-ball" array, which subtends 4π steradians. Finally, we choose a very fast detector so that successive pulses, mostly from the radioactive decay, will be registered separately rather than piling up.

2 Calculational Approach

The detector response to neutrons and gamma rays was studied using the Monte Carlo code GEANT 3.21. [GEA95] Since the final decision about the crystal size is different from the previous simulatations, all the new simulations are made with the actual geometry. The inner radius of a closed sphere in the following simulations is 17 cm instead of 10 cm in all the previous simulations. [Hei99],[Hei01]

Compared with the previous approach, the handling of inelastic neutron scattering on barium was improved. Additionally every setup was simulated eight times with initial neutron energies from different energy decades so that the influence of high energetic neutrons to later time of flight was easier to investigate.

During the simulations done in 1999, it turned out that the number of clusters formed during a single event offers better opportunities than the number of hit crystals to distinguish between events caused by neutron capture on the sample and events due to captures after scattering on the sample. Therefore spectra with cuts on the cluster multiplicity are included for each present simulation.

2.1 Information contained in resulting .hbook files

The results of the GEANT simulations are retained on files suitable for further analysis. They are saved in the so called hbook-type, which is used by the CERN software package PAW for data analysis and graphical display.

2.1.1 γ-response

Table 1 gives the .hbook data files for the response of the full array to gamma rays.

Spectrum Content
1 total energy deposited in the crystal ball
5 multiplicity distribution
6 cluster multiplicity distribution
7 energy deposition in sample
8 energy deposition beam pipe and moderator
9 2D spectrum: detector- vs. event multiplicity
10 2D spectrum: cluster- vs. event multiplicity
11 .. 35 total energy for multiplicities 1 .. 25
41 .. 65 total energy for cluster multiplicities 1 .. 25
101 .. 262 energy deposited in crystal 1 .. 162

Table 1: Description of spectra created for γ-simulations.

2.1.2 Neutron response

Table 2 gives the .hbook files for the response of the full array to neutrons.

Spectrum	Content	Event type
1	total energy deposited in the crystal ball	all
2	2D spectrum : total energy vs. TOF	capture
3	2D spectrum : total energy vs. TOF	scatter
4	interaction time in crystal ball	all
5	multiplicity distribution	all
6	cluster multiplicity distribution	all
7	energy deposition in beam pipe and moderator	all
8	energy deposition in sample	all
9	total energy deposited in the crystal ball	capture
10 .. 11	2D spectrum : total energy vs. TOF	capture
12 .. 13	2D spectrum : total energy vs. TOF	scatter
14 .. 15	neutron spectrum	all

Continued next page

16
multiplicity distribution
capture

17
cluster multiplicity distribution
capture

21 .. 45
total energy for multiplicities 1 .. 25
capture

46 .. 60
total energy for cluster multiplicities 1 .. 15
capture

61 .. 85
total energy for multiplicities 1 .. 25
scatter

86 .. 100
total energy for cluster multiplicities 1 .. 15
scatter

101 .. 262
energy deposited in crystal 1 .. 162
all

301 .. 320
total energy for TOF intervals (10^{-3}, 10^{-2}) .. (10^{16}, 10^{-17}) eV
capture

351 .. 370
total energy for TOF intervals (10^{-3}, 10^{-2}) .. (10^{16}, 10^{-17}) eV
scatter

Table 2: Description of spectra created for neutron simulations.

2.2 Geometry

The modeled detector consists of 162 BaF_2 crystals of 15 cm length. Covering the full solid angle without any gaps requires four different crystal shapes, which can be seen in Figure 1. The shapes of the crystals are optimized in a way that they all cover the same solid angle, although they have different shapes [Hab79].

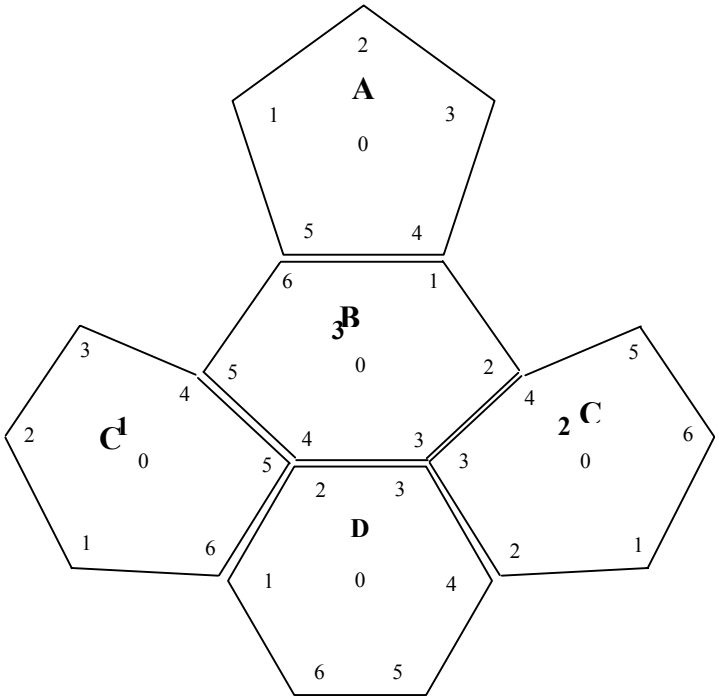

Figure 1: The detector is composed of 12 crystals of type A, 60 crystals of type B, 60

Table 3 shows the dimensions of the 4 crystal shapes. See Figure 1 for definitions of the line segments.

Table 3: Dimensions of the different crystal shapes for a 4π array of unit radius.

Line Segment	Type			
	A	B	C	D
12	0.21436	0.17624	0.19423	0.17442
23	0.21436	0.16630	0.17501	0.17442
34	0.21436	0.17358	0.16622	0.17442
45	0.21436	0.16630	0.16622	0.17442
56 (51 for A)	0.21436	0.17624	0.17501	0.17442
61	-	0.21428	0.19423	0.17442
10	0.18234	0.18000	0.15055	0.17442
20	0.18234	0.20783	0.17596	0.17442
30	0.18234	0.14331	0.20455	0.17442
40	0.18234	0.14331	0.15055	0.17442
50	0.18234	0.20783	0.20455	0.17442
60	-	0.18000	0.17596	0.17442

The volumes described above can be arranged to form a closed sphere with an inner radius of 17 cm and an outer radius of 32 cm. In the present simulation, however, the crystals were moved outwards by 0.66 cm and the resulting gaps of 2 mm between the crystals were filled with a mixture of aluminum, Teflon and air to simulate materials used to reflect the scintillation light at the surfaces and to isolate each crystal from its neighbors. The mixture is equivalent to 0.1 mm aluminum foil, 0.5 mm Teflon and 0.4 mm air surrounding every crystal. The front of the crystal is also covered with aluminum and Teflon. Figure 2 shows the model of the detector with all crystals.

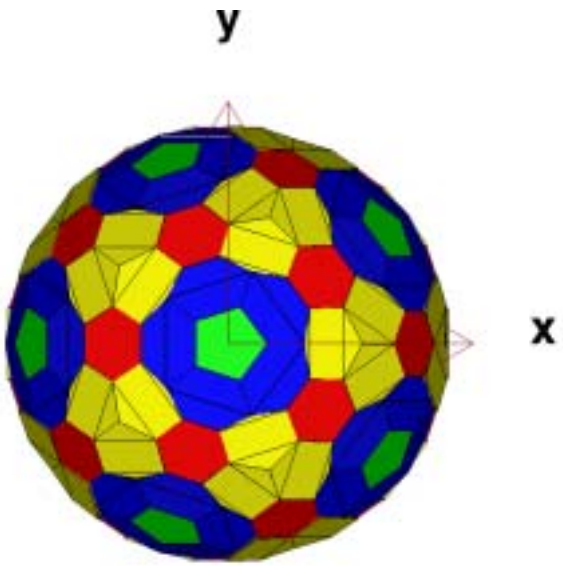

Figure 2: Model of the detector with all 162 BaF_2 crystals.

3 Detector response for γ-rays

3.1 Mono-energetic γ's

3.1.1 Mono-energetic γ's started in the center of the BaF_2 array

With the geometry described in section 2.2 the detector response for randomly distributed γ-rays with energies from 0.25 MeV up to 20 MeV emitted in the center of the BaF_2 crystal ball was investigated. Figure 3, Figure 4, and Figure 5 show the resulting multiplicity and cluster multiplicity distributions and the sum energy spectra for 100,000 initial γ-rays of each energy. For γ-energies below 4.5 MeV multiplicity 1 is most abundant and for energies between 4.5 and 20 MeV multiplicity 2 is the most abundant, whereas the most likely cluster multiplicity for all γ-energies is 1. This means that the cluster multiplicity of an event is more suitable to deduce the number of the initial γ-ray than the multiplicity. A cluster is defined as adjoining crystals where energy is deposited in the event.

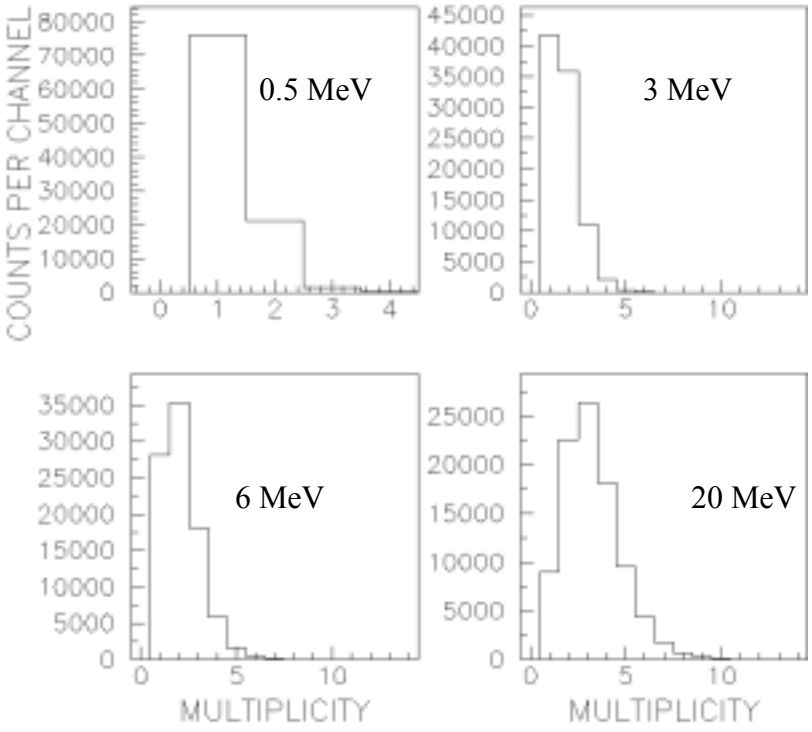

Figure 3: Multiplicity distribution for γ-energies 0.5, 3, 6 and 20 MeV started in the center of the BaF_2 crystal ball.

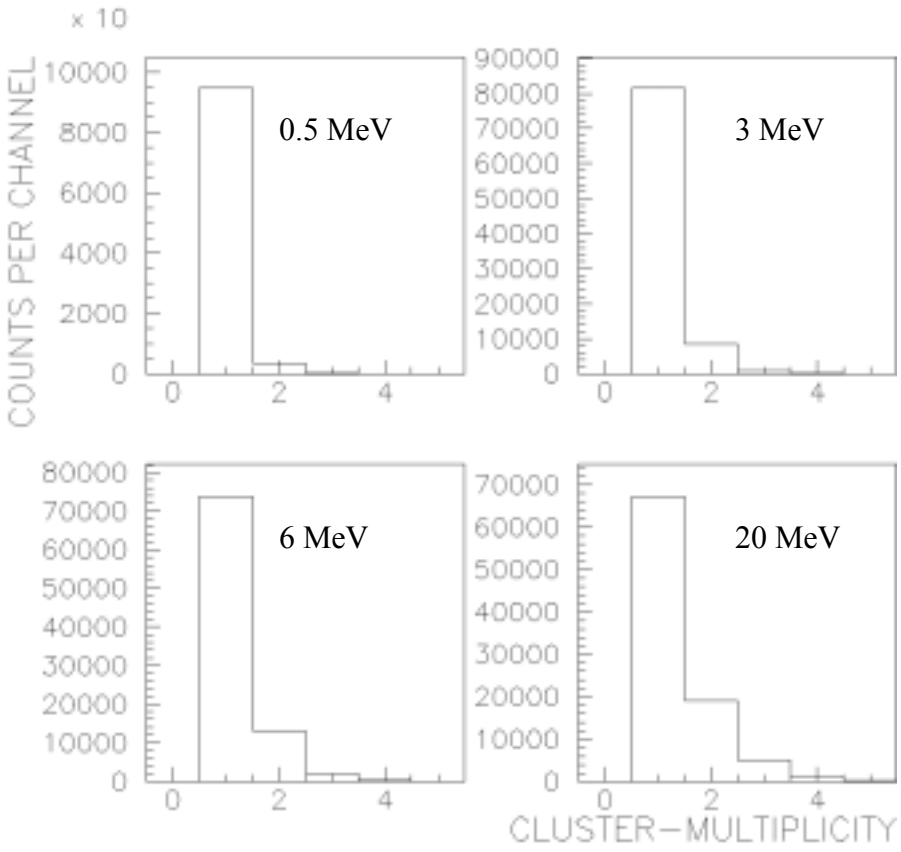

Figure 4: Cluster-multiplicity distribution for γ-energies energies 0.5, 3, 6 and 20 MeV started in the center of the BaF_2 crystal ball.

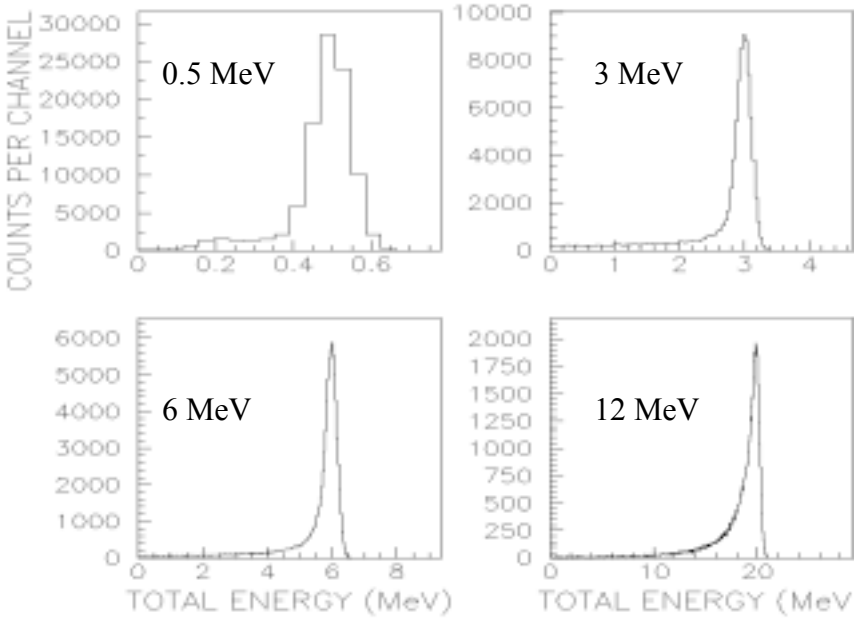

Figure 5: Energy deposit summed over all crystals for γ-energies from 0.5, 3, 6, 20 MeV. For each calculation, 100,000 initial photons were tracked.

Total efficiency, average multiplicity, and average cluster multiplicity as a function of γ-energy are given in Table 4. Only the standard energy cut-off at 50 keV was applied for the calculation of the total efficiency. The average multiplicity as a function of gamma-ray energy is shown in Figure 6.

Table 4: Total γ-ray efficiency (fraction of γ-rays depositing any energy above 50 keV in the BaF_2 array), multiplicity, and cluster multiplicity for 160 crystals as a function of E_γ.

γ-energy (MeV)	total efficiency in %	Av. multiplicity	Av. cluster multiplicity
0.25	99	1.07	1.03
0.5	98	1.24	1.04
1.0	97	1.42	1.05
2.0	93	1.57	1.07
3.0	91	1.72	1.12
4.0	90	1.86	1.15
5.0	90	1.98	1.18
6.0	89	2.09	1.21
7.0	89	2.17	1.23
8.0	90	2.25	1.24
9.0	90	2.36	1.26
10.0	91	2.45	1.28
15.0	92	2.89	1.33
20.0	93	3.24	1.36

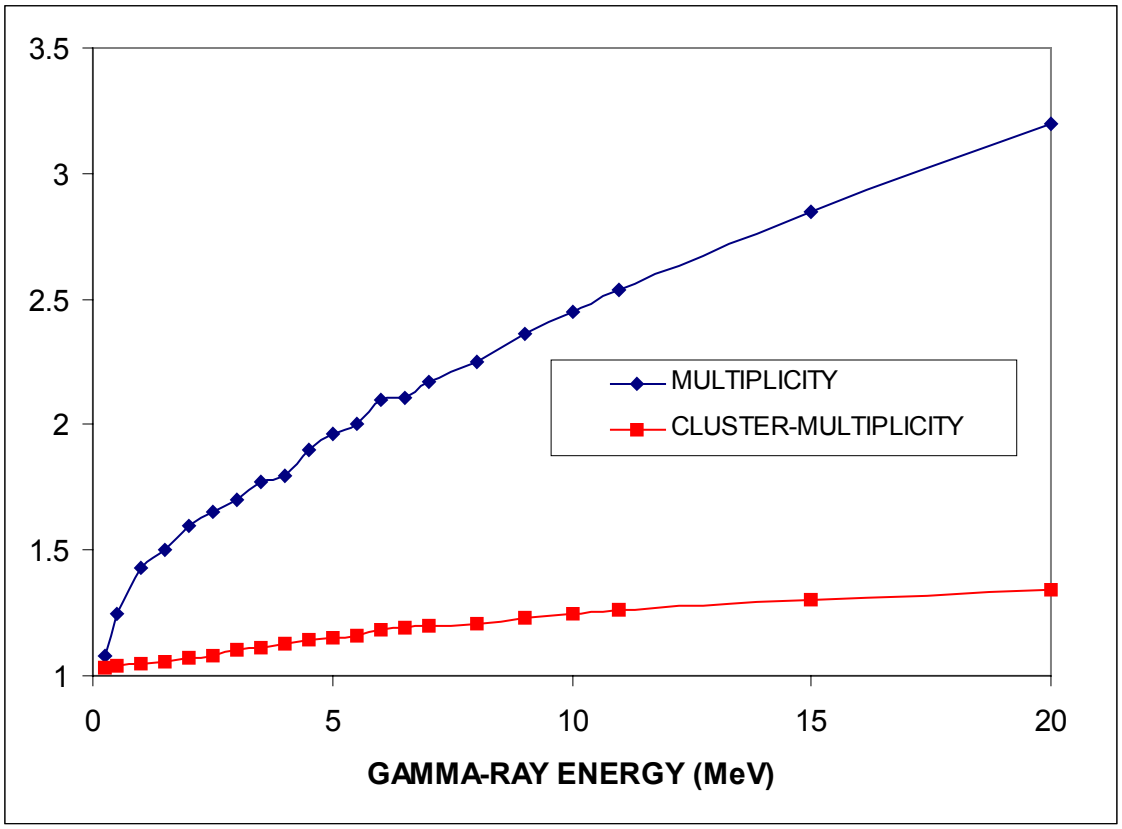

Figure 6: Average multiplicity versus primary γ-ray energy.

3.1.2 Mono-energetic γ's from outside of the BaF_2 array

With the geometry used before and an additional aluminum sphere (R_i = 49.7 cm, R_o = 53.5 cm) as well as a combined structure of PM and supporting for the PM, the response for γ-rays with energies from 0.25 MeV up to 20 MeV was investigated. The γ-rays were perpendicularly emitted from a disk (R = 55 cm) outside of the BaF_2 crystal ball (Figure 7). Figure 8, Figure 9, and Figure 10 show the resulting sum energy spectra and multiplicity distributions for 100,000 initial γ-rays of each energy. Most of the events have a cluster multiplicity of 1. Since also other background components tend to have small cluster multiplicity (neutron capture at barium, α-activity of crystals) no additional cut needs to be applied in order to discriminate these events. In order to estimate the count rate in the BaF_2-array caused by γ-rays from outside the crystal ball, one just needs to estimate the total number of gammas (independent of the direction) entering a sphere of 55 cm radius and multiply by the efficiency given below.

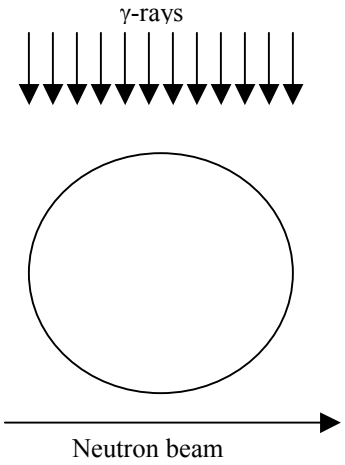

Figure 7: Schematic view of the simulation setup

Table 5: Total γ-ray efficiency, multiplicity, and cluster multiplicity for 160 crystals as a function of E_γ.

γ-energy (MeV)	total efficiency in %	Av. multiplicity	Av. cluster multiplicity
0.25	31	1.03	1.02
0.5	34	1.1	1.02
1.0	36	1.3	1.03
2.0	38	1.5	1.07
3.0	39	1.5	1.09
4.0	40	1.6	1.11
5.0	40	1.7	1.12
6.0	41	1.7	1.13
7.0	42	1.8	1.14
8.0	43	1.8	1.15
9.0	43	1.9	1.17
10.0	44	2.0	1.18
15.0	46	2.3	1.24
20.0	48	2.7	1.29

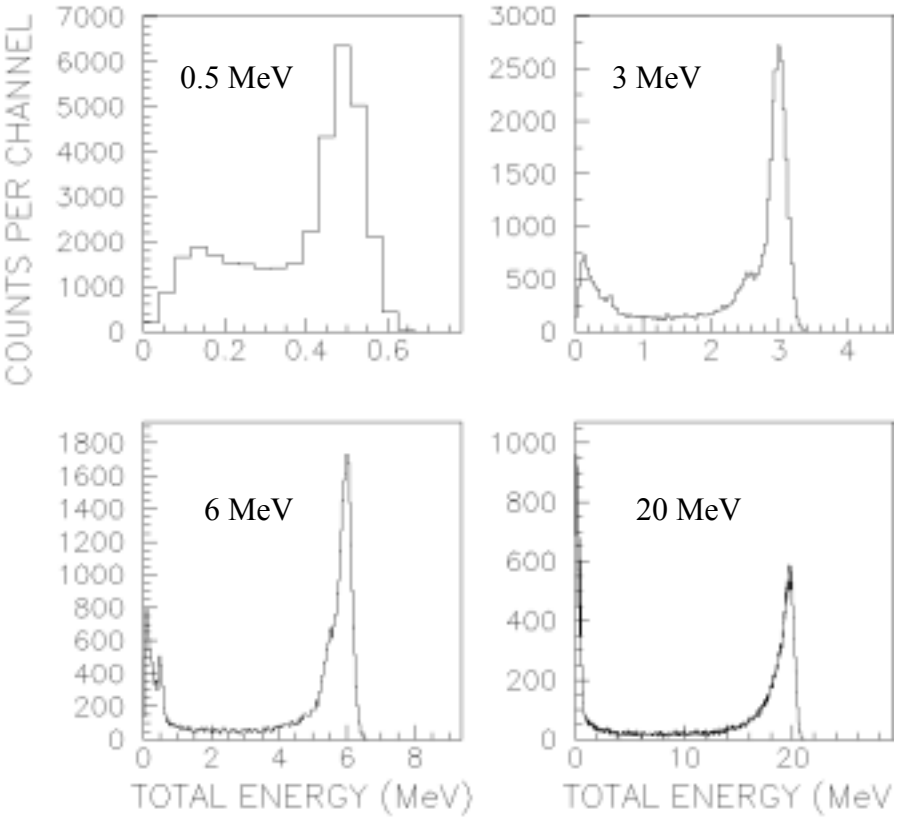

Figure 8: Energy deposit summed over all crystals for γ-energies 0.5, 3, 6, 20 MeV incident from outside the BaF2 crystal ball. For each calculation, 100,000 initial photons were tracked.

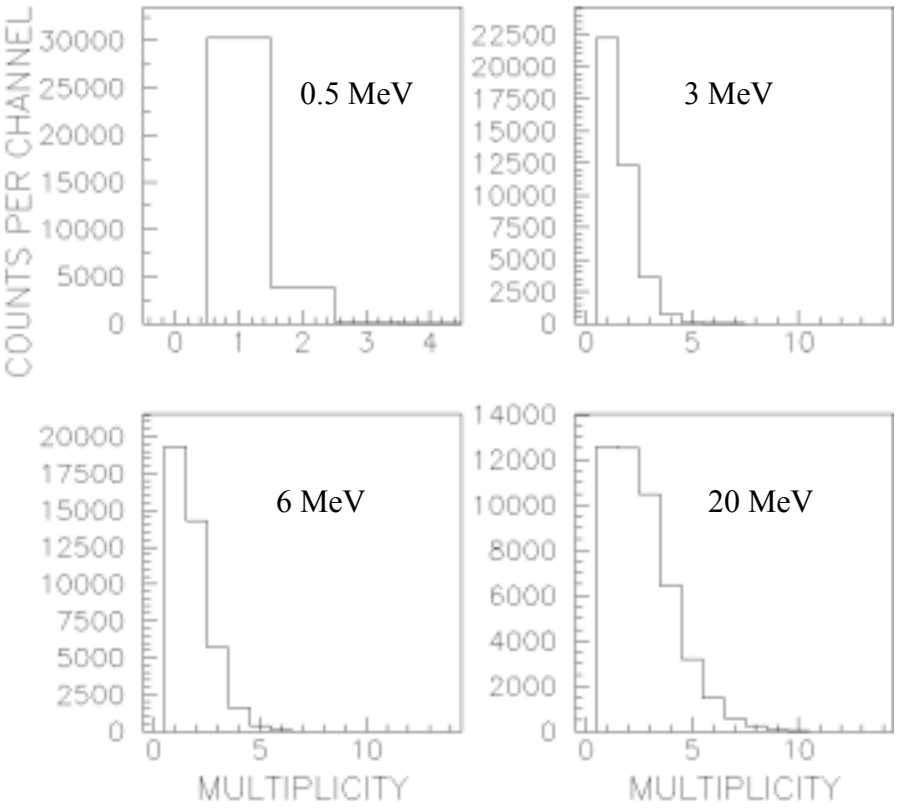

Figure 9: Multiplicity distribution for γ-energies 0.5, 3, 6, 20 MeV started outside the BaF_2 crystal ball.

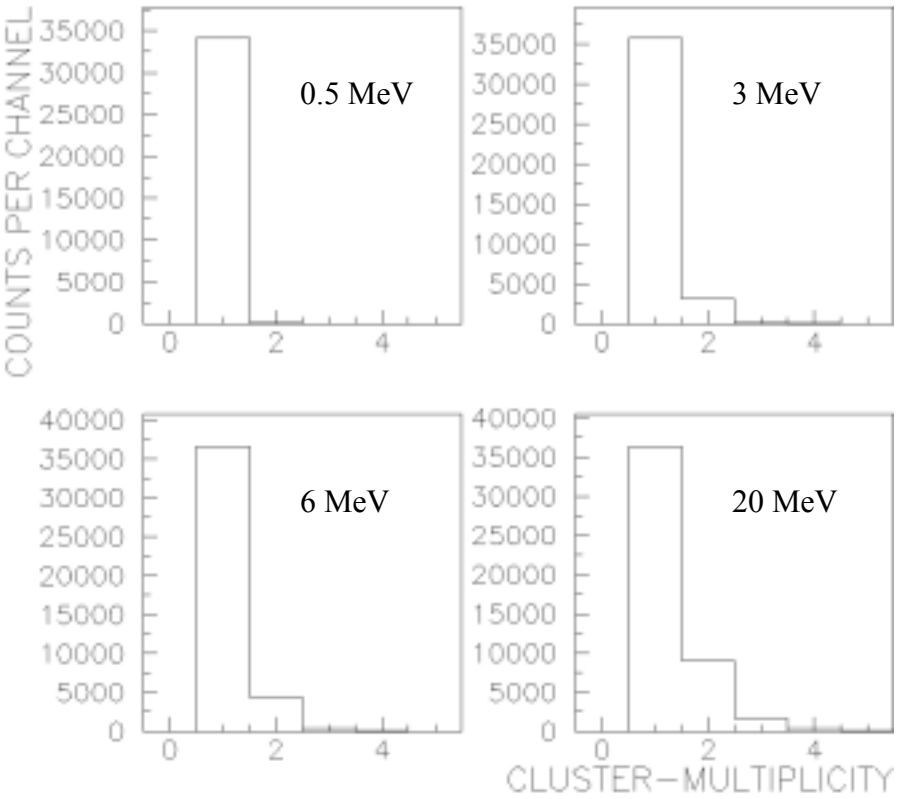

Figure 10: Cluster multiplicity distribution for γ-energies 0.5, 3, 6, 20 MeV started outside of the BaF_2 crystal ball.

3.1.3 Mono-energetic γ's and a single shielded (Compton-suppressed) crystal

The production of all the BaF_2 crystals will take at least one year. During this period only a part of the whole sphere is available, and it is important to know if a partial array would be useful. The simulations done with a single pentagonal crystal that is vetoed by its neighboring hexagonal crystals will show that even for this small number of detectors reasonable measurements can be done. The first test was the response to mono-energetic γ-rays in the energy range from 0.25 up to 20 MeV. There were 2 mm gaps between the crystals filled with a composition of 1 mm air, 0.2 mm aluminum, and 0.8 mm Teflon. The crystals were placed at the same positions as if they would form part of a 4π array (
Figure 11).

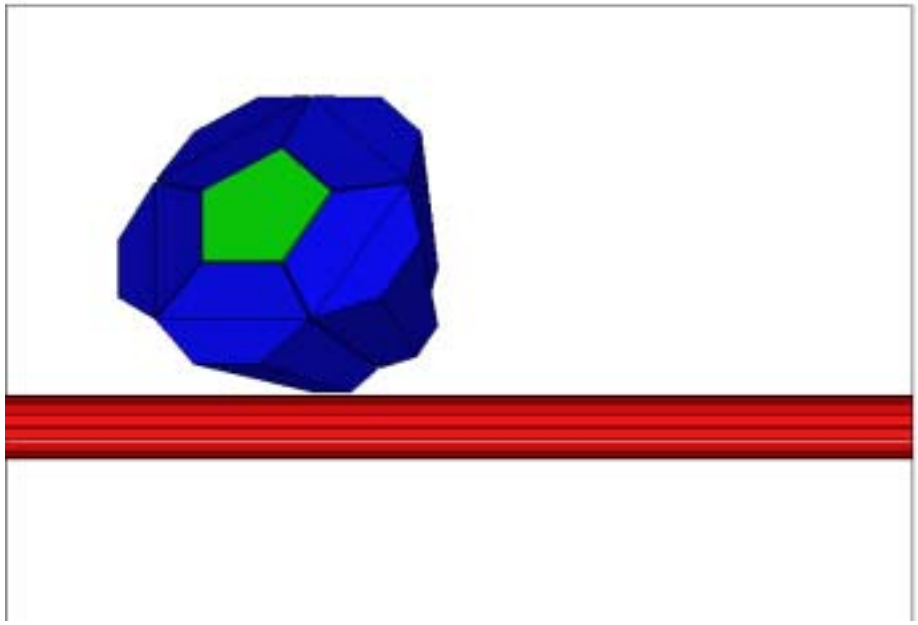

Figure 11: Setup used for simulations. One pentagonal crystal (green) is surrounded by 5 hexagonal crystals (blue). Whenever energy in one of the hexagons is deposited, the event is vetoed.

Due to the small solid angle covered by one single crystal (0.62 % of 4π), 1,000,000 initial gammas were necessary in order to get reasonable statistics. The total efficiency as well as the peak efficiency as a function of γ-ray energy for this geometry are summarized in Table 6. Spectra of the energy deposited in the single pentagonal crystal vetoed by surrounding hexagonal crystals are shown in Figure 12.

Table 6: Total (counts above 50 keV) and peak (counts above 90 % of E_γ) efficiency for a single pentagon vetoed by 5 surrounding hexagonal crystals as a function of E_γ.

γ-energy (MeV)	total efficiency (%)	Peak efficiency (%)
0.25	0.62	0.62
0.5	0.52	0.42
1.0	0.42	0.32
2.0	0.38	0.27
3.0	0.33	0.19
4.0	0.29	0.18
5.0	0.26	0.14
6.0	0.25	0.13
7.0	0.24	0.12
8.0	0.22	0.12
9.0	0.20	0.12
10.0	0.18	0.12
15.0	0.14	0.06
20.0	0.10	0.04

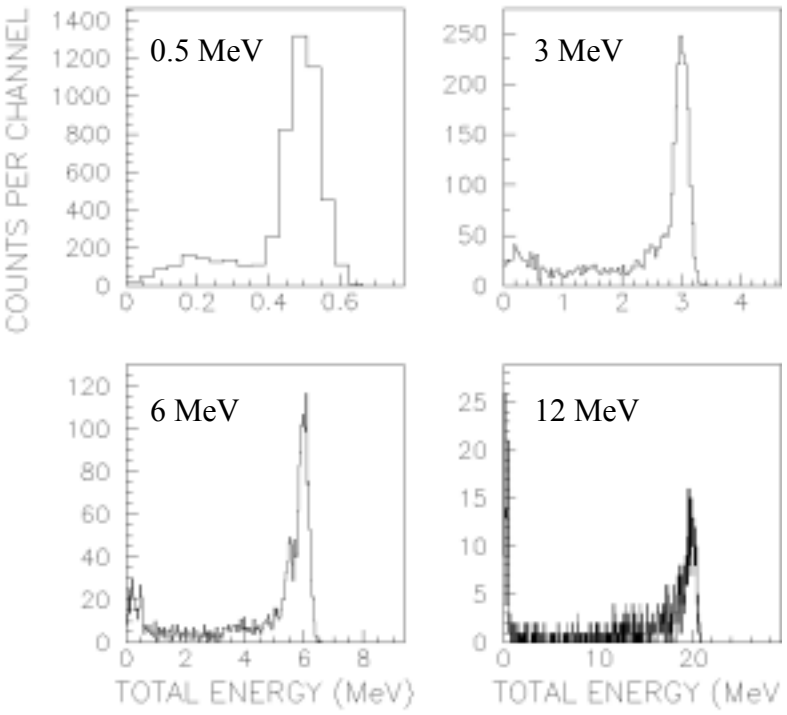

Figure 12: Energy deposit in the single vetoed crystal crystals for γ-energies from 0.5, 3, 6, 20 MeV. For each calculation, 1,000,000 initial photons were tracked.

3.2 γ-cascades from neutron capture in ^{197}Au

The response of the detector for the ^{197}Au(n,γ)^{198}Au reaction (Q = 6.512 MeV) was also simulated. For ^{198}Au an isomer exists with a lifetime of 124 ns at 0.312 MeV. For neutron capture events populating this isomer the prompt energy is reduced to 6.200 MeV plus the energy of the incoming neutron. The decay into the ground state as well as the decay of the ground state itself are not taken into consideration. For the simulation theoretical γ-cascades for capture of 100 keV neutrons calculated by Uhl [Uhl93a,Uhl93b] were used, which have multiplicities of at most 7. Again 100,000 events were simulated. The average multiplicity of detectors firing for the full crystal ball was 4.9, the average cluster multiplicity 3.4. The total efficiency was 99.8 %.

3.2.1 Effect of beam pipe

To get realistic simulations, two opposite pentagonal crystals were left out for an aluminum beam pipe with 5 cm outer diameter and different wall thickness. The beam pipe consists of aluminum and the effect of beam pipe thickness was investigated. These results show that a degradation of the spectra becomes significant for aluminum beam pipes of more than 3 mm wall thickness.

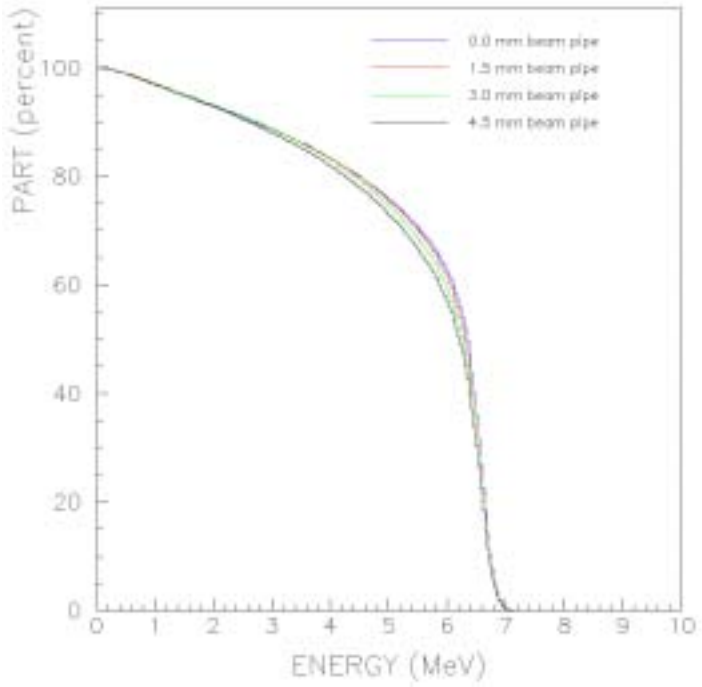

Figure 13: Percentage of counts above a given threshold energy for different beam pipe thicknesses.

3.2.2 Different moderator thickness

Neutron simulations with a gold sample showed, that the background due to neutrons scattered on the sample and finally captured on the surrounding material can be significantly reduced by using a ^{6}LiH moderator/absorber around the sample. In order to investigate the influence of such a moderator/absorber to the response to γ-cascades following a neutron capture on ^{197}Au, simulations with 160 BaF_2 crystals, an aluminum beam pipe (R_i = 2.3 cm, R_a = 2.5 mm), 2mm gaps between the crystals filled with a mixture of air, Teflon and aluminum, and gold cascades started in the center of the crystal ball were made. Figure 14 shows the part of events above a given energy for different moderator thicknesses.

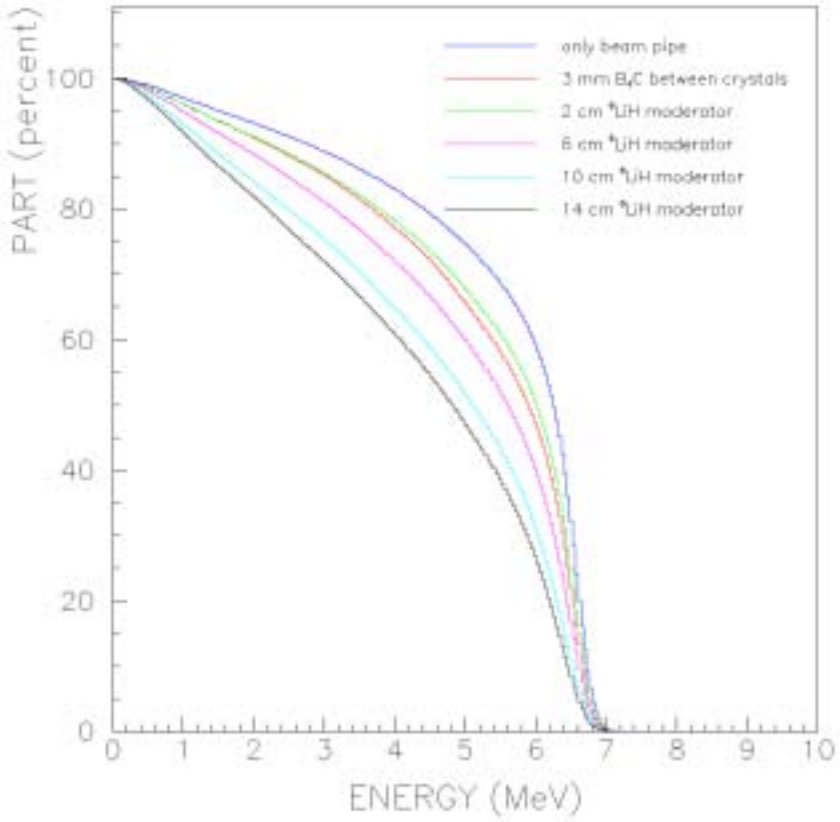

Figure 14: Influence of moderator/absorber thickness on the shape of the gold peak (for detailed description, see section 4.2). Plotted is the percentage of counts above a given threshold energy.

3.2.3 Different absorbing Materials between crystals

The most efficient way of reducing the background signals caused by scattered neutrons is a combination of moderator material around the capture sample and neutron absorbing material between the BaF_2 crystals. In order to keep the flexibility for choosing different thicknesses of absorbing materials, the gaps between the crystals were increased to 4 mm. This small change in geometry causes already a significant reduction of the full energy peak (Figure 15). A detailed description of all the different setups is given in section 4.2.

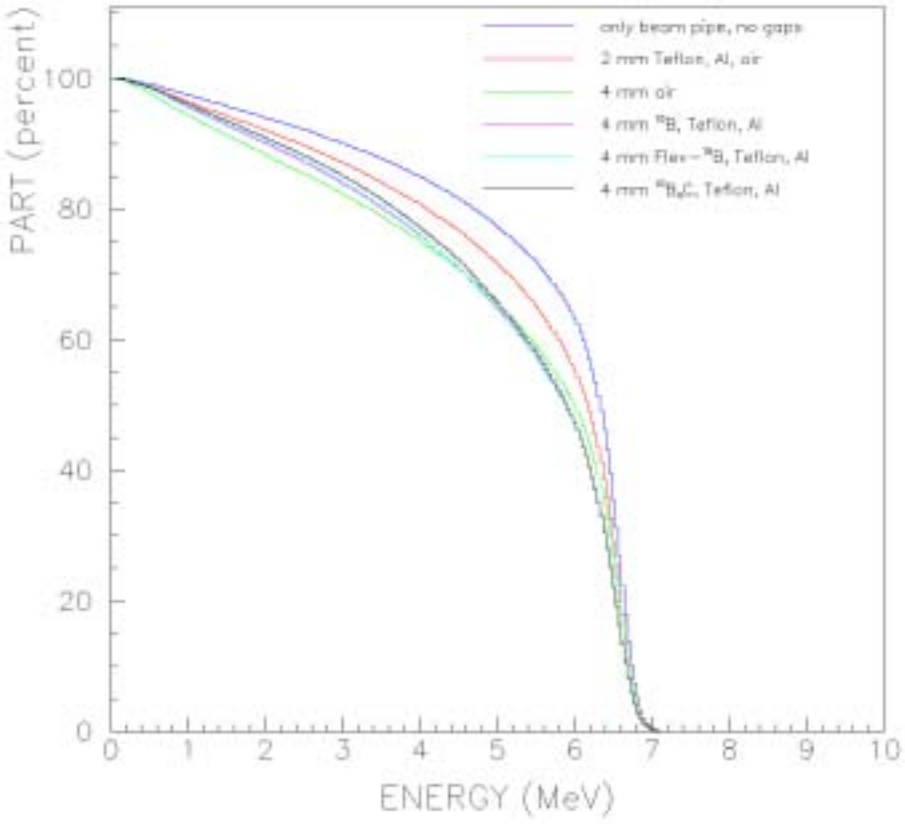

Figure 15: Percentage of counts above a given threshold energy for different absorber materials for gold cascades. In order to see the effect of the missing solid angle due to gaps between crystals one simulation was made with just 4 mm air and no heavier material between the crystals.

3.2.4 Gold cascades and a single shielded (Compton-suppressed) crystal

In order to check the response to gold cascades simulations of a vetoed crystal in the same position as in the full sphere were done. The total efficiency is 1.4 %, that is 1.4% of the captures produce a non-vetoed signal. Since the γ-multiplicity of the event is usually greater than one, there exist the possibility that the actual event is not vetoed due to Compton scattering, single escape or similar effects, but due to interaction of a second γ-ray with the anti-coincidence detectors surrounding the central detector. This means, that the efficiency for detecting a γ-ray decreases with multiplicity because the veto-probability increases. For gold cascade with an average multiplicity of about 4 this effect is about 10 %. There are different possibilities to handle this problem. The easiest way avoiding it, is to decrease the detection efficiency by increasing the distance to the sample. Another opportunity would be to shield the veto-crystals with high-Z material that should have a very low (n,γ)-cross section.

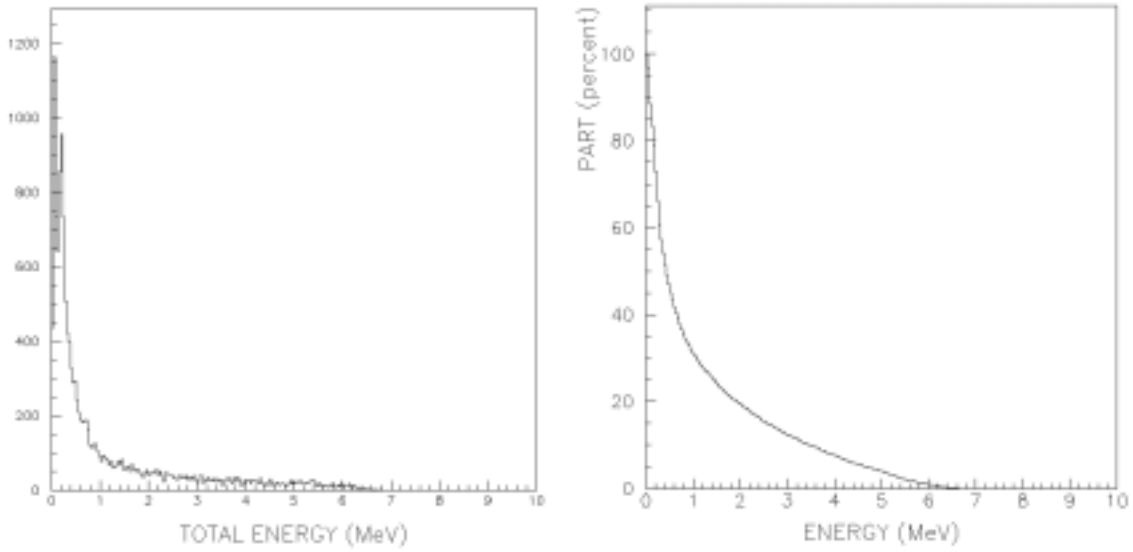

Figure 16: Response of a single vetoed crystal to γ-cascades following a neutron capture on ^{197}Au. The left part shows counts vs. energy and the right part shows the same date as percentage of counts above a given threshold energy.

4 Simulations with neutrons

4.1 Neutron spectrum

A fit of the measured data of Figure 17 gave a neutron spectrum for Flight Path 4 of the form

$$\log_{10}(\text{flux})=3.07-0.948\ \log_{10}(E_n)$$

but for simplicity a spectrum following $1/E_n$ was assumed for the simulations. For neutron energies E_n > 100 keV the spectrum has not been measured. The neutron spectrum at the new flight path, FP14, is expected to have the same shape as is shown in Figure 18. The simulations showed that neutrons of energies between 8 MeV and 12 MeV could be important because the (n,2n) and the (n,3n) channels for ^{138}Ba and ^{197}Au open at 8 MeV and have cross sections of about 2 barns. Neutrons produced in these reactions have lower energies and are likely captured in the crystals, causing considerable background. In addition, such capture events appear in the TOF spectrum at later times and when primary neutrons of somewhat lower energy are just arriving at the sample. Simulations showed, however, that this effect is not significant for a neutron spectrum of the form $1/E_n$. So far, little is known about the true spectrum above 100 keV, but quantitative information would be required for assessing effects if the spectrum deviates from $1/E$ at these higher energies. For the simulations neutrons with energies between 1 eV and 100 MeV were assumed to have a $1/E_n$ dependence up to 20 MeV and to be constant above 20 MeV.

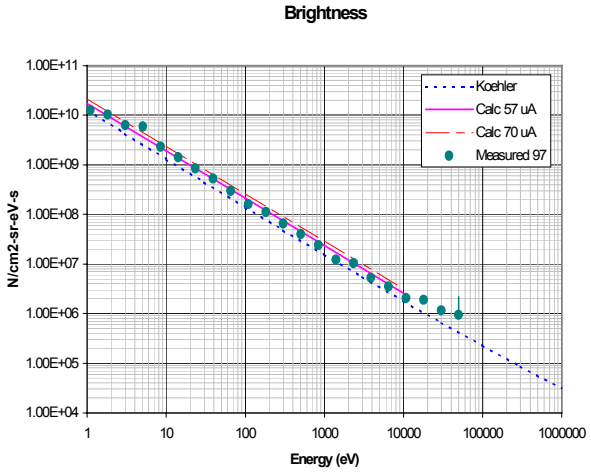

Figure 17: Calculated and measured brightness for the previous flight path (FP4).

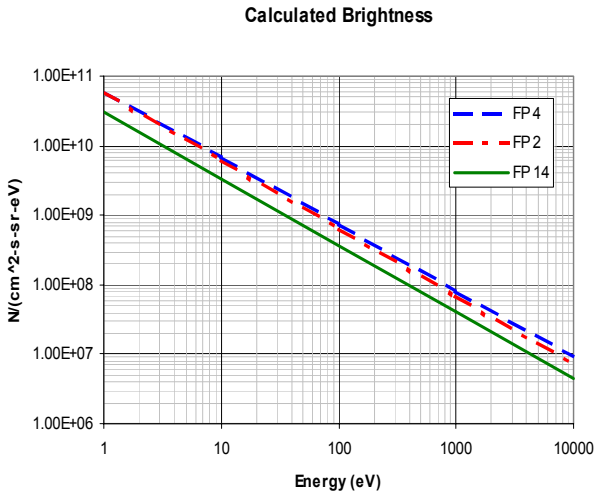

Figure 18: Calculated brightness on the new flight paths (FP14) and on a flight path used for a short time previously (FP2).

4.2 Time-of-flight (TOF) spectra

The following calculations were done with a flight path of 20 m neglecting the pulse width of the proton beam that drives the MLNSC spallation neutron source and also neglecting the moderation time of neutrons in the source. To save computing time a rather thick gold sample (1 mm thick, 1 cm in diameter) was used for the simulations. This should not effect the ratio between scattered and captured neutrons of interest, while the γ-ray attenuation in the sample can still be tolerated. A geometry with 160 crystals of 15 cm length, aluminum and Teflon between the crystals and a beam pipe with an inner diameter of 4.4 cm and an outer diameter of 5.0 cm was used.

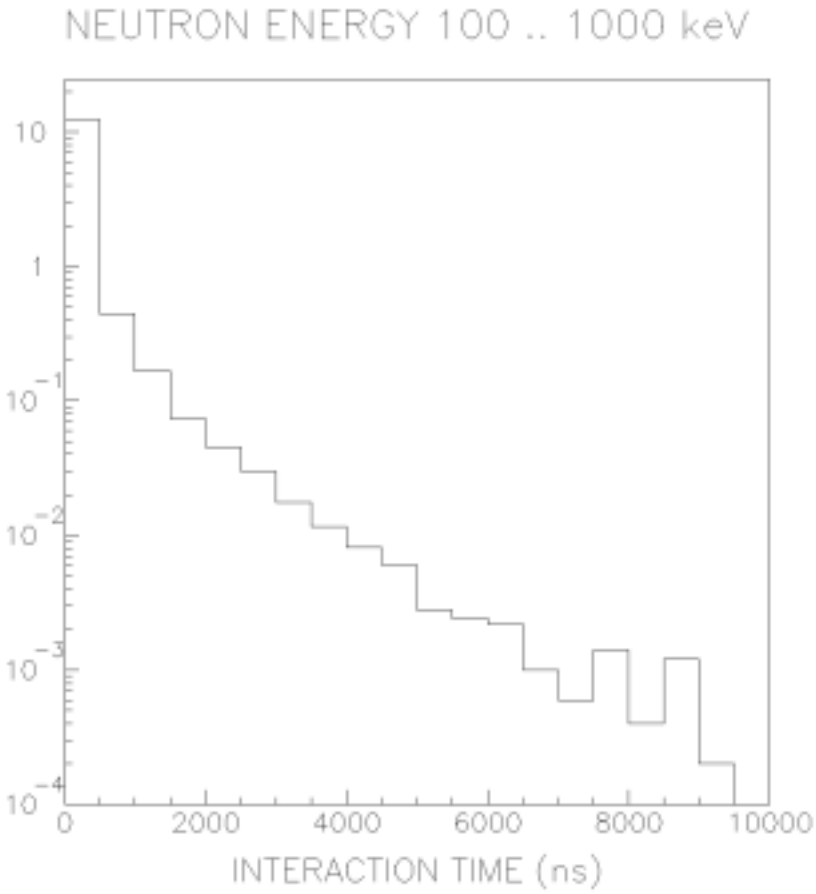

Figure 19: Distribution of interaction time in the BaF_2 sphere for neutrons with initial energies between 0.1 and 1 MeV.

In order to handle the high background count rate due to radioactive samples, it might be necessary to require short coincidence times. Figure 19 shows the interaction time distribution for initial neutrons between 0.1 and 1 MeV. Note especially that events due to scattered neutrons can be as long as 10 μs after scattering from the sample. If the initial energies were above the threshold for inelastic scattering, this means that by applying short coincidence time cuts, one would split such events into more than one event.

4.2 Background from scattered neutrons

In this section, the possibilities to decrease the ratio of detected scattered neutrons to neutrons captured in the 1 mm thick, 1 cm diameter gold sample in the energy region from 1 keV to 1 MeV are discussed for different BaF_2 arrays. Descriptions of the different experimental setups are as follows:

1. **STANDARD** setup with 160 crystals of 15 cm length with aluminum and Teflon between the crystals and an aluminum beam pipe (R_i = 2.2 cm, R_a = 2.5 cm), supporting structure with PM-emulation (mixture of Al, Ni, Fe and Cu) as discussed above.
2. as discussed above.
3. standard without supporting structure & PM
4. standard with 30% ^{10}Borated polyethylene between PM
5. standard with spherical ^{6}LiH (ρ = 0.85 g/cm^3) moderator (R_i = 2.5 cm, R_a = 10.5 cm) around sample
6. standard with 3 mm Flex-^{10}Boron (ρ = 1.64 g/cm^3, 26.9 % Fe, 25.4 % ^{10}B, 24.1 % O, 20.1 % C, 2.8 % H), 0.2 mm Al, 0.8 mm Teflon between crystals (and half in front)
7. standard with 3 mm Flex-^{10}Boron and 8 cm ^{6}LiH moderator (4 & 5)
8. standard with 3 mm Flex-^{10}Boron and 11 cm ^{6}LiH moderator (R_i = 5 cm, R_a = 16cm)
9. standard with 3 mm $^{10}B_4C$ + binder (ρ = 1.22 g/ cm^3, 28 % ^{10}B, 40 % C, 28 % O, 4 % H), 0.2 mm Al, 0.8 mm Teflon between crystals (and half in front)
10. standard with 3 mm $^{10}B_4C$ and 8 cm ^{6}LiH moderator (R_i = 2.5 cm, R_a = 10.5 cm)
11. standard with 3 mm $^{10}B_4C$ and 11 cm ^{6}LiH moderator (R_i = 5 cm, R_a = 16cm)
12. standard with 3 mm ^{10}B (ρ = 2.0 g/cm^3), 0.2 mm Al, 0.8 mm Teflon between crystals (and half in front)
13. standard with 3 mm ^{10}B and 8 cm ^{6}LiH moderator (R_i = 2.5 cm, R_a = 10.5 cm)
14. standard with 3 mm ^{10}B and 11 cm ^{6}LiH moderator (R_i = 5 cm, R_a = 16cm)
15. standard with 3 mm ^{6}LiF (ρ = 2.63 g/ cm^3), 0.2 mm Al, 0.8 mm Teflon between crystals (and half in front)
16. standard with 3 mm ^{6}LiF and 6 cm ^{6}LiH moderator (R_i = 2.5 cm, R_a = 8.5 cm)
17. standard with 3 mm ^{6}LiF and 8 cm ^{6}LiH moderator (R_i = 2.5 cm, R_a = 10.5 cm)
18. standard with 3 mm ^{6}LiF and 11 cm ^{6}LiH moderator (R_i = 5 cm, R_a = 16cm)
19. standard with 3 mm ^{6}LiF and 11 cm ^{6}LiH moderator (R_i = 2.5 cm, R_a = 13.5 cm)
20. single vetoed crystal (description see 4.5)

The results are summarized in Table 7.

Table 7: Ratio of events from scattered neutrons and true capture for different setups for events with E_{tot} > 1 MeV (except 19b).

Setup	Ratio between scattered and captured events for different neutron energy regions.			
	0.1 .. 1 keV	1 ..10 keV	10 .. 100 keV	0.1 .. 1 MeV
1 standard	0.82	1.44	2.77	5.24
2 no supporting structure	0.58	1.14	1.72	1.98
3 30% ^{10}Borated ployethylene between PM	0.80	1.44	2.77	5.3
4 8 cm ^{6}LiH around beam pipe (sph)	0.24	0.32	1.17	3.3
5 3 mm Flex-^{10}Boron between crystals	0.19	0.49	1.69	3.84
6 3mm Flex-^{10}Boron, 8 cm ^{6}LiH	0.074	0.15	0.78	2.3
7 3mm Flex-^{10}Boron, 11 cm ^{6}LiH	0.074	0.13	0.68	2.3
8 3 mm $^{10}B_4C$ between crystals	0.23	0.58	1.63	3.6
9 3 mm $^{10}B_4C$, 8 cm ^{6}LiH	0.087	0.17	0.76	2.2
10 3 mm $^{10}B_4C$, 11 cm ^{6}LiH	0.087	0.15	0.67	2.0
11 3 mm ^{10}B between crystals	0.043	0.37	0.67	1.8
12 3 mm ^{10}B, 8 cm ^{6}LiH	0.042	0.081	0.41	1.3
13 3 mm ^{10}B, 11 cm ^{6}LiH	0.044	0.078	0.35	1.07
14 3 mm ^{6}LiF between crystals	0.27	0.65	1.67	3.5
15 3 mm ^{6}LiF, 5 cm ^{6}LiH	0.10	0.20	0.93	2.3
16 3 mm ^{6}LiF, 8 cm ^{6}LiH	0.10	0.18	0.82	2.2
17 3 mm ^{6}LiF, 11 cm ^{6}LiH	0.093	0.16	0.72	1.9
18 3 mm ^{6}LiF, 11 cm ^{6}LiH (inner shell)	0.10	0.17	0.75	1.9
19a single vetoed crystal, events > 1 MeV	0.073	0.11	0.28	0.36
19b single vetoed crystal, all events	0.038	0.063	0.15	30

From item 13 of this table, it is apparent that including a ^{6}LiH shell around the sample and ^{10}B between the crystals results in about a factor of 10 improvement in the scattered-to-capture ratio in the neutron energy range of 10- 100 keV, of great interest for astrophysics.

In summary, the best solution is obtained by filling the gaps between the crystals with ^{10}B and by using a moderator/absorber made of ^{6}LiH around the beam pipe.

4.3 Background from neutrons coming from outside

In section 3.1.2 the response to gammas coming from outside have been investigated. In the planned setup also neutrons due to scattering processes at walls and from other experiments might enter the BaF_2 volume. The detection efficiency and the detector response for such events were simulated. The actual response is not different from the response to neutrons scattered at the sample inside the array. The typical structure with different peaks according to captures on different barium isotopes remains. This means all the techniques to handle the neutron-induced background using energy and multiplicity cuts will work fine also for events due to neutrons coming from outside the crystal ball. The simulated geometry is the same as in section 3.1.2. In order to estimate the induced count rate in the detector it is sufficient to know the number and energy of neutrons entering a spherical volume of radius 55 cm. Multiplying this number with the efficiency listed in Table 8 gives the total number of events expected.

Table 8: Total efficiency for neutrons of different energy ranges entering the BaF_2 array from outside.

neutron energy	ε_{tot} (%)
1 ..10 eV	7.3
10 .. 100 eV	2.1
0.1 .. 1 keV	3.0
1 ..10 keV	2.3
10 .. 100 keV	2.0
0.1 .. 1 MeV	1.6
1 ..10 MeV	2.6
10 .. 100 MeV	2.0

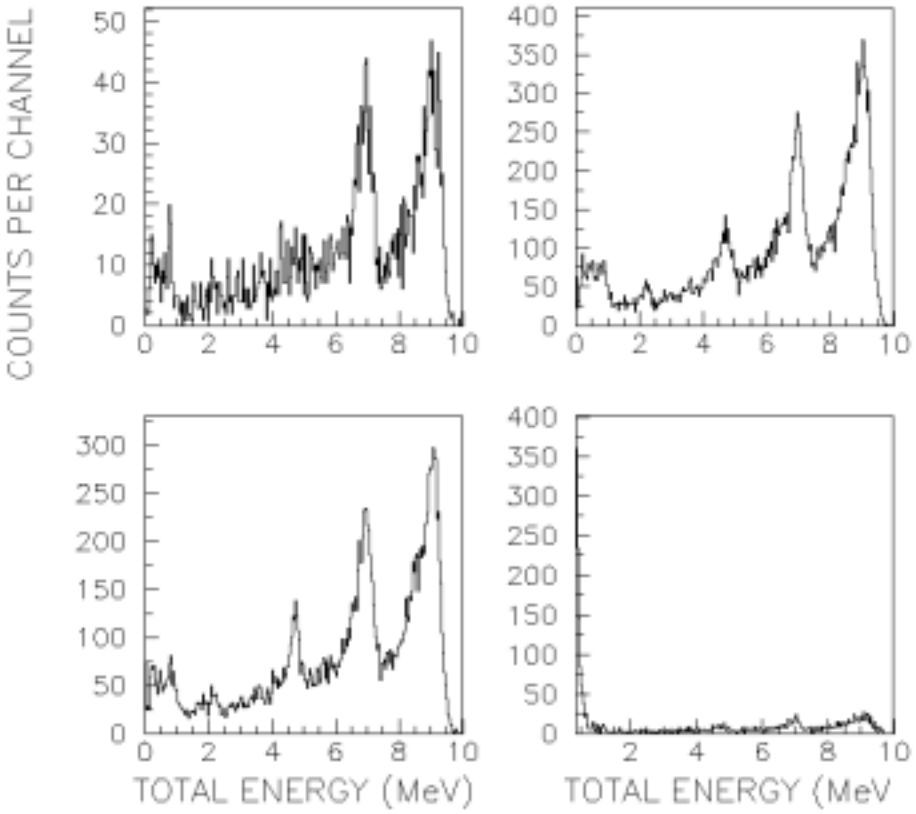

Figure 20: Total energy distribution for neutrons coming from outside the crystal ball. The initial neutron energy was 0.1 - 1 keV (left, top), 1 - 10 keV (right, top), 10 - 100 keV (left, bottom) and 0.1 - 1 MeV (right, bottom).

4.4 Hit pattern

The hit pattern from captured and scattered events may also carry important information. Since most of the possible cuts would depend on the properties of the individual isotope, only the general cut on cluster multiplicity was under investigation. Figure 24 shows the comparison of cluster multiplicity distribution of real capture events on a gold sample and capture events in the BaF_2 crystals after neutron scattering on the gold sample. Even for neutron energies around 1 MeV a cut in cluster multiplicity of 3 would be sufficient to have a signal to background ratio of better than 1.

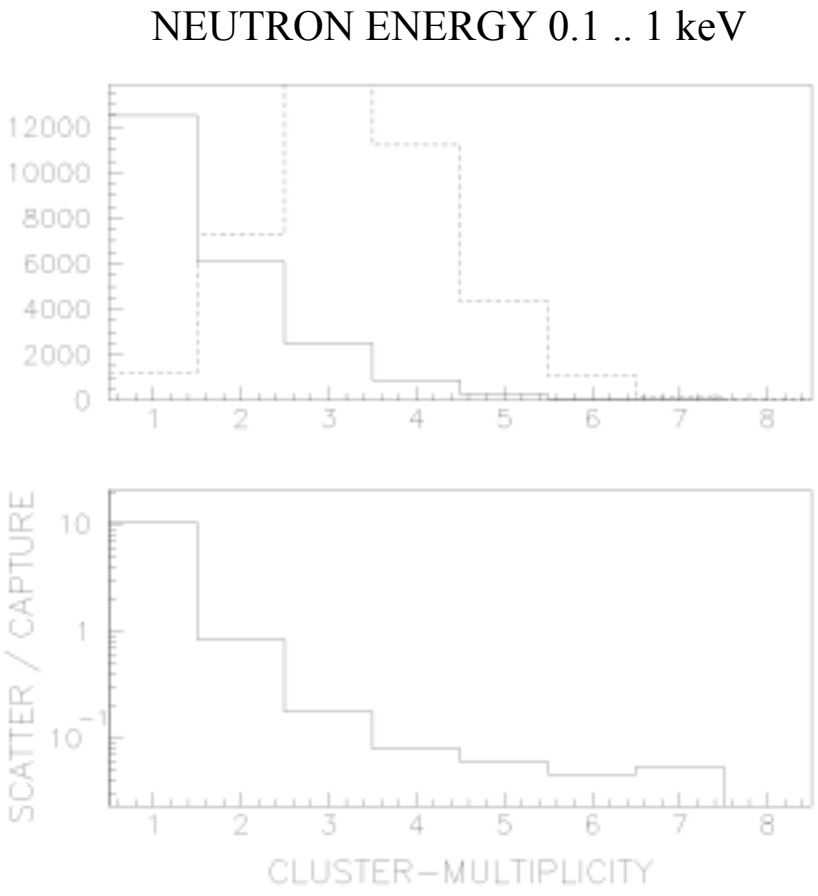

Figure 21: Cluster multiplicity distribution for events from scattered neutrons captured in BaF_2 (solid) and for true capture events in a gold sample (dashed) are shown in the top figures. The bottom figures show the ratio (background / signal) between the two multiplicity distributions. The initial neutron energies were 0.1 – 1 keV.

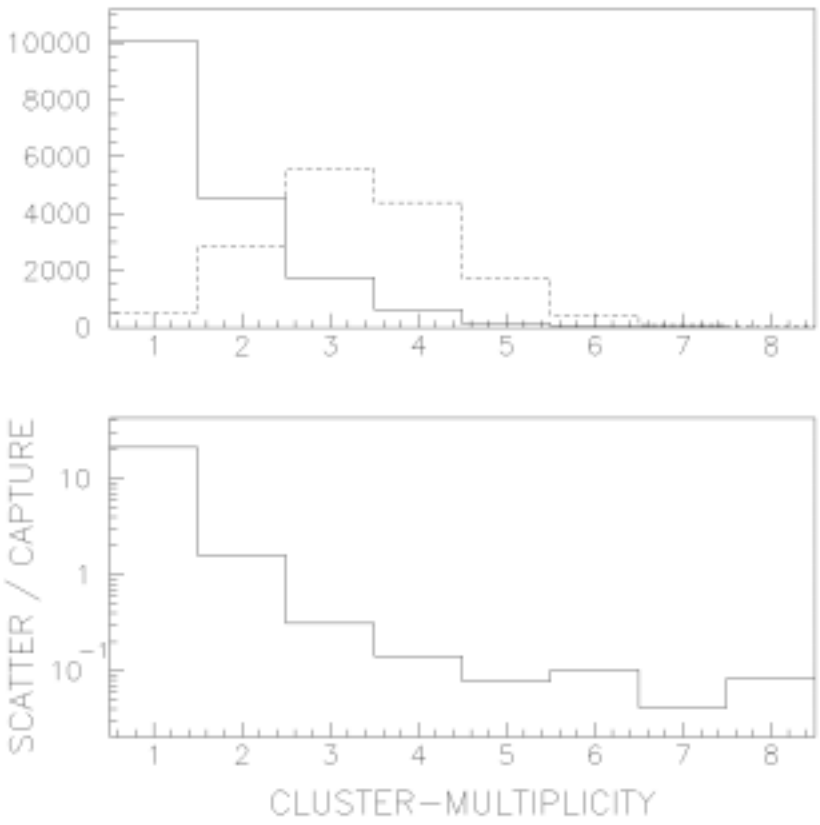

Figure 22: Cluster multiplicity distribution for events from scattered neutrons captured in BaF_2 (solid) and for true capture events in a gold sample (dashed) are shown in the top figures. The bottom figures show the ratio (background / signal) between the two multiplicity distributions. The initial neutron energies were 1 – 10 keV.

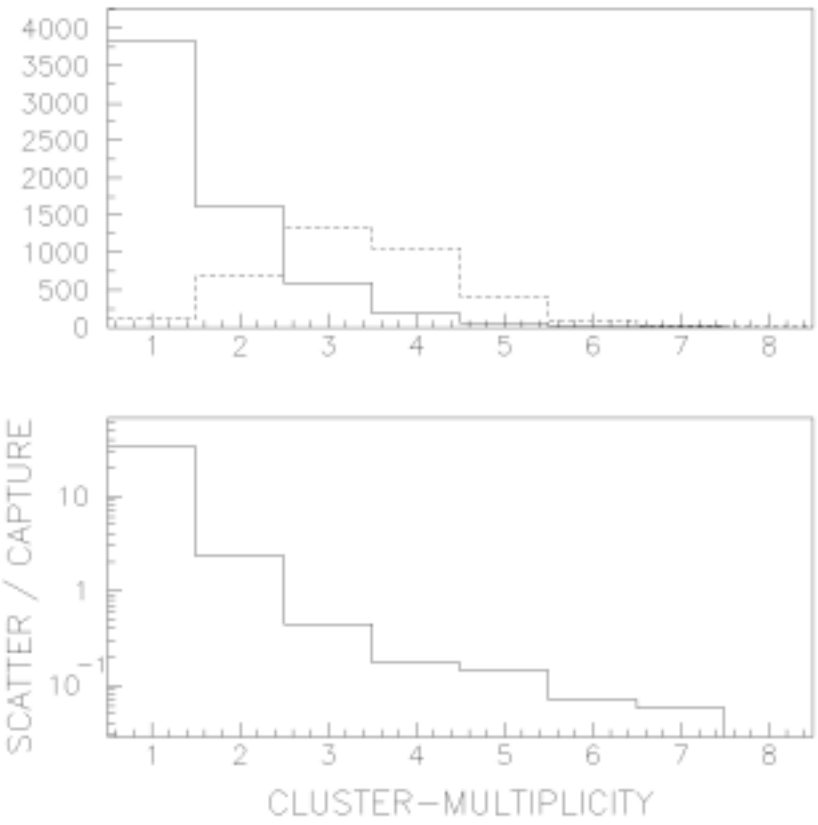

Figure 23: Cluster multiplicity distribution for events from scattered neutrons captured in BaF_2 (solid) and for true capture events in a gold sample (dashed) are shown in the top figures. The bottom figures show the ratio (background / signal) between the two multiplicity distributions. The initial neutron energies were 10 – 100 keV.

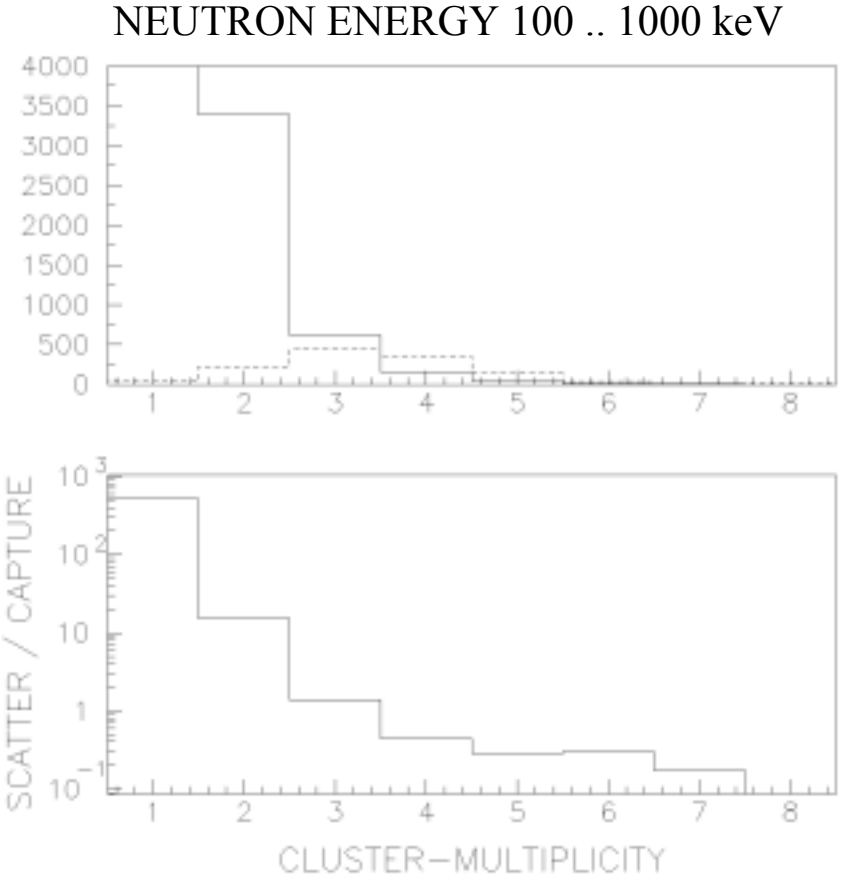

Figure 24: Cluster multiplicity distribution for events from scattered neutrons captured in BaF_2 (solid) and for true capture events in a gold sample (dashed) are shown in the top figures. The bottom figures show the ratio (background / signal) between the two multiplicity distributions. The initial neutron energies were 0.1 – 1 MeV.

4.5 Neutron response of a single shielded crystal

Since most of the neutron-capture events in the single crystal would deposit energy in one of the neighboring crystals, most of the background due to scattered neutrons is discriminated by the veto shielding. An additional effect of the veto is that the background due to captures on barium still keeps the energy distribution of the full crystal ball. If there is no energy deposition in the surrounding crystals, there is a very high probability for depositing all the released energy in the single crystal. Only neutron captures close to the front or the rear of the quite long, tapered crystals can loose energy without a veto from the surrounding crystals. This offers additional opportunities for discriminating the neutron-induced background.

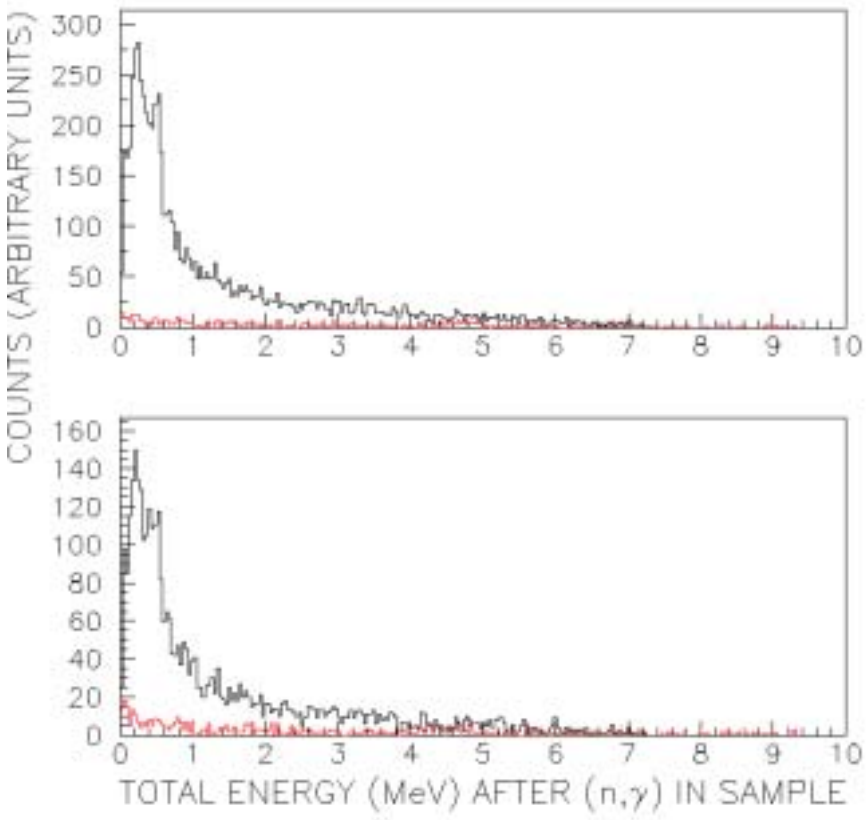

Figure 25: Neutron response of a single crystal (pentagon) vetoed by 5 crystals (hexagon) around it. The black line corresponds to events due to captures on a gold sample, the red curve to events due to neutrons scattered at the gold sample. The neutron energy range was 1 - 10 keV (top) and 10 -100 keV (bottom).

5 Conclusions

These calculations for the geometry that is being built as the DANCE detector can be compared with the results of calculations for a smaller-size, bare detector (10 cm inner radius, 25 cm outer radius) [Hei99], [Hei01] as follows:

- The response to gamma rays is unchanged
- Neutron absorbing material between crystals is somewhat less efficient than for smaller diameter
- The aluminum supporting has significant influence
- First measurements can be done with small BaF_2 arrays

6 References

[GEA95] GEANT - Detector Description and Simulation Tool, Simone Giani and Sven Ravndal , CERN (1995).

[Hab79] D. Habs, F. S. Stephens and R. M. Diamond, "A Proposal for a Crystal Ball System," *Lawrence Berkeley Laboratory report* LBL-8945 (1979).

[Hei99] M. Heil, R. Reifarth, F. Kaeppeler, K. Wisshak, F. Voss, J. L. Ullmann, R. C. Haight, E. H. Seabury, J. B. Wilhelmy, R. S. Rundberg and M. M. Fowler, "GEANT Simulations of Neutron Capture Experiments with a 4π BaF_2 Detector", *Los Alamos National Laboratory report* LA-UR-99-4096 (1999).

[Hei01] M. Heil, R. Reifarth, M.M. Fowler, R.C. Haight, F. Kaeppeler, R.S. Rundberg, E.H. Seabury, J.L. Ullmann, J.B. Wilhelmy, K. Wisshak, "A 4π BaF_2 Detector for (n,γ) Cross Section Measurements at a Spallation Source", *Nucl. Inst. Meth*. **A459** (2001) 229.

[Uhl93a] M. Uhl and J. Kopecky, "Neutron capture cross section and gamma ray strength functions" in Nuclei in the Cosmos, eds. F. Kaeppeler and K. Wisshak (IOP, Bristol, 1993), pp. 259-266.

[Uhl93b] M. Uhl private communications (1993).

7 Appendix

In the following tables a short description for all the runs simulated is given. Simulations with mono energetic γ-rays are summarized in Table 9. The runs with gold cascades are listed in Table 10. The simulations of neutron response of the array to neutrons scattered from the 1 mm thick ^{197}Au sample are given in Table 11.

Table 9: Description of simulations with mono energetic gamma rays

Run	geometry	E_γ
1	160 crystal, Teflon, aluminum	0.25
2		0.5
3		1.0
4		1.5
5		2.0
6		2.5
7		3.0
8		3.5
9		4.0
10		4.5
11		5.0
12		5.5
13		6.0
14		6.5
15		7.0
16		8.0
17		9.0
18		10
19		11
20		15
21		20
50	160 crystal, Teflon, aluminum, Al-beam pipe	0.25
51		0.5
52		1.0
53		1.5
54		2.0
55		2.5
56		3.0
57		3.5
58		4.0
59		5.0
60		6.0
61		10
62		15
63		20
123	160 crystal, Teflon, aluminum, Al-beam pipe, Al-supporting, 2 mm in front, 4 mm between B_4C, Teflon, Aluminum	0.25
124		0.5
125		1.0
126		1.5
127		2.0
128		2.5
129		3.0
130		3.5
131		4.0
132		4.5
133		5.0
134		6.0
135		7.0
136		8.0
137		9.0

138		10
139		15
140		20
300	1 vetoed crystal	0.25
301		0.5
302		1.0
303		1.5
304		2.0
305		2.5
306		3.0
307		4.0
308		6.0
309		10
310		15
311		20
321		5.0
322		7.0
323		8.0
324		9.0

Table 10: Description of simulations with cascades after (n,γ) on ^{197}Au

Run	geometry
22	160 crystal, Teflon, aluminum
49	160 crystal, Teflon, aluminum, Al-beam pipe (3 mm)
88	160 crystal, Teflon, aluminum, Al-beam pipe (1.5 mm)
89	160 crystal, Teflon, aluminum, Al-beam pipe (4.5 mm)
115	160 crystal, no gaps, 1mm Au sample
116	160 crystal, 2 mm Teflon, Aluminum
117	160 crystal, 2 mm in front, 4 mm between B_4C, Teflon, Aluminum, 1mm Au sample
118	160 crystal, 2 mm in front, 4 mm between ^{10}B, Teflon, Aluminum, 1mm Au sample
119	160 crystal, 2 mm in front, 4 mm between Flex-^{10}B, Teflon, Aluminum, 1mm Au sample
120	160 crystal, 0 mm in front, 4 mm between B_4C, Teflon, Aluminum, 1mm Au sample
121	160 crystal, 0 mm in front, 4 mm between ^{10}B, Teflon, Aluminum, 1mm Au sample
122	160 crystal, 0 mm in front, 4 mm between Flex-^{10}B, Teflon, Aluminum, 1mm Au sample
182	160 crystal, 2 mm Teflon, Aluminum, 2 cm ^{6}LiH moderator, 1mm Au sample
183	160 crystal, 2 mm Teflon, Aluminum, 4 cm ^{6}LiH moderator, 1mm Au sample
184	160 crystal, 2 mm Teflon, Aluminum, 6 cm ^{6}LiH moderator, 1mm Au sample
185	160 crystal, 2 mm Teflon, Aluminum, 8 cm ^{6}LiH moderator, 1mm Au sample
186	160 crystal, 2 mm Teflon, Aluminum, 10 cm ^{6}LiH moderator, 1mm Au sample
187	160 crystal, 2 mm Teflon, Aluminum, 12 cm ^{6}LiH moderator, 1mm Au sample
188	160 crystal, 2 mm Teflon, Aluminum, 14 cm ^{6}LiH moderator, 1mm Au sample
189	160 crystal, 2 mm Teflon, Aluminum, 11 cm ^{6}LiH moderator (outer shell) , 1mm Au sample
198	160 crystal, 0 mm in front, 4 mm between Teflon, Aluminum, 1mm Au sample
199	160 crystal, 0 mm in front, 4 mm between air, 1mm Au sample
200	160 crystal, 0 mm in front, 0 mm between (no gaps)
201	160 crystal, 0 mm in front, 4 mm between, air
202	160 crystal, 0 mm in front, 2 mm between, air
203	160 crystal, 1 mm in front, 2 mm between Teflon, Aluminum
204	160 crystal, 2 mm in front, 4 mm between, Flex-Boron
205	160 crystal, 2 mm in front, 4 mm between, B_4C
206	160 crystal, 2 mm in front, 4 mm between, ^{10}B
210	160 crystal, 2 mm Teflon, Aluminum, 2 cm ^{6}LiH moderator
211	160 crystal, 2 mm Teflon, Aluminum, 4 cm ^{6}LiH moderator
212	160 crystal, 2 mm Teflon, Aluminum, 6 cm ^{6}LiH moderator
213	160 crystal, 2 mm Teflon, Aluminum, 8 cm ^{6}LiH moderator
214	160 crystal, 2 mm Teflon, Aluminum, 10 cm ^{6}LiH moderator
215	160 crystal, 2 mm Teflon, Aluminum, 12 cm ^{6}LiH moderator
216	160 crystal, 2 mm Teflon, Aluminum, 14 cm ^{6}LiH moderator
217	160 crystal, 2 mm Teflon, Aluminum, 11 cm ^{6}LiH moderator (outer shell)
312	1 vetoed crystal

Table 11: Description of simulations of neutron response on 1 mm ^{197}Au sample

Run	geometry	log(E_n / V)
23	160 cryst.	5 (mono)
24 .. 32	160 cryst.	1 .. 9
33 .. 40	160 cryst., Al-beam pipe, Al-supporting	1 .. 8
41 .. 48	160 cryst., Al-beam pipe	1 .. 8
64 .. 71	160 cryst., Al-beam pipe, Al-supporting, 30 % BPE between PM	1 .. 8
72 .. 79	160 cryst., Al-beam pipe, Al-supporting, 3 mm Flex-B	1 .. 8
80 .. 87	160 cryst., Al-beam pipe, Al-supporting, 8 cm ^{6}LiH	1 .. 8
91 .. 98	160 cryst., Al-beam pipe, Al-supporting, 3 mm Flex-B, 8 cm ^{6}LiH	1 .. 8
99 .. 106	160 cryst., Al-beam pipe, Al-supporting, 3 mm Flex-B, 11 cm ^{6}LiH	1 .. 8
107 .. 114	160 cryst., Al-beam pipe, Al-supporting, 4 mm B_4C	1 .. 8
141 .. 148	160 cryst., Al-beam pipe, Al-supporting, neutrons from outside	1 .. 8
150 .. 157	160 cryst., Al-beam pipe, Al-supporting, 3 mm B_4C	1 .. 8
158 .. 165	160 cryst., Al-beam pipe, Al-supporting, 3 mm B_4C, 8 cm ^{6}LiH	1 .. 8
166 .. 173	160 cryst., Al-beam pipe, Al-supporting, 3 mm B_4C, 11 cm ^{6}LiH	1 .. 8
174 .. 181	160 cryst., Al-beam pipe, Al-supporting, 3 mm ^{10}B	1 .. 8
190 .. 197	160 cryst., Al-beam pipe, Al-supporting, 3 mm ^{10}B, 11 cm ^{6}LiH	1 .. 8
220 .. 227	160 cryst., Al-beam pipe, Al-supporting, 3 mm ^{10}B, 8 cm ^{6}LiH	1 .. 8
228 .. 235	160 cryst., Al-beam pipe, Al-supporting, 3 mm B_4C, 8 cm ^{6}LiH	1 .. 8
236 .. 243	160 cryst., Al-beam pipe, Al-supporting, 3 mm ^{6}LiF	1 .. 8
244 .. 251	160 cryst., Al-beam pipe, Al-supporting, 3 mm ^{6}LiF, 8 cm ^{6}LiH	1 .. 8
252 .. 259	160 cryst., Al-beam pipe, Al-supporting, 3 mm ^{6}LiF, 11 cm ^{6}LiH (outer shell)	1 .. 8
260 .. 267	160 cryst., Al-beam pipe, Al-supporting, 3 mm ^{6}LiF, 11 cm ^{6}LiH	1 .. 8
268 .. 275	160 cryst., Al-beam pipe, Al-supporting, 3 mm ^{6}LiF, 6 cm ^{6}LiH	1 .. 8
313 .. 320	1 vetoed crystal	1 .. 8